HHS Public Access

Author manuscript

Exp Eye Res. Author manuscript; available in PMC 2023 January 01.

Published in final edited form as:

Exp Eye Res. 2022 January ; 214: 108894. doi:10.1016/j.exer.2021.108894.

Effect of Long-term Chronic Hyperhomocysteinemia on Retinal Structure and Function in the Cystathionine-β-Synthase Mutant Mouse

Haiyan Xiao, PhD[1,2], **Jing Wang, PhD**[1,2], **Shannon R. Barwick, BS**[1,2], **Yisang Yoon, PhD**[2,3], **Sylvia B. Smith, PhD**[1,2,4]

[1]Department of Cellular Biology and Anatomy, Medical College of Georgia, Augusta University, Augusta, GA.

[2]James and Jean Culver Vision Discovery Institute, Augusta University, Augusta, GA.

[3]Department of Physiology, Medical College of Georgia, Augusta University, Augusta, GA.

[4]Department of Ophthalmology, Medical College of Georgia, Augusta University, Augusta, GA

Abstract

Elevated levels of the excitatory amino acid homocysteine (Hcy) have been implicated in retinal diseases in humans including glaucoma and macular degeneration. It is not clear whether elevated Hcy levels are pathogenic. Models of hyperhomocysteinemia (Hhcy) have proven useful in addressing this including mice with deficiency in the enzyme cystathionine β-synthase (CBS). *Cbs*$^{+/-}$ mice have a ~two-fold increase in plasma and retinal Hcy levels. Previous studies of visual function and structure in *Cbs*$^{+/-}$ mice during the first 10 months of life revealed mild ganglion cell loss, but minimal electrophysiological alterations. It is not clear whether extended, chronic exposure to moderate Hhcy elevation will lead to visual function loss and retinal pathology. The present study addressed this by performing comprehensive analyses of retinal function/structure in 20 month *Cbs*$^{+/-}$ and *Cbs*$^{+/+}$ (WT) mice including IOP, SD-OCT, scotopic and photopic ERG, pattern ERG (pERG), and visual acuity. Eyes were harvested for histology and immunohistochemical analysis of Brn3a (ganglion cells), dihydroethidium (oxidative stress) and GFAP (gliosis). The analyses revealed no difference in IOP between groups for age/strain. Visual acuity measured ~0.36c/d for mice at 20 months in *Cbs*$^{+/-}$ and WT mice; contrast sensitivity did not differ between groups at either age. Similarly SD-OCT, scotopic/photopic ERG and pERG revealed no differences between 20 month *Cbs*$^{+/-}$ and WT mice. There was minimal disruption in retinal structure when eyes were examined histologically. Morphometric analysis revealed no significant differences in retinal layers. Immunohistochemistry revealed ~5 RGCs/100μm retinal length in both *Cbs*$^{+/-}$ and WT mice at 20 months. While there was greater oxidative stress and

*Please send correspondence to: Sylvia B. Smith, Ph.D., Department of Cellular Biology and Anatomy, Medical College of Georgia, Augusta University, 1120 15th Street, CB 1114, Augusta, GA 30912-2000, 706-721-7392 (phone), 706-721-6120 (fax), sbsmith@augusta.edu.

Declaration of competing interest

None.

Appendix A. Supplementary Data

Supplementary data are available for this study.

gliosis in older (20 month) mice versus young (4 month) mice, there was no difference in these parameters between the 20 month *Cbs*$^{+/-}$ and WT mice. We conclude that chronic, moderate Hhcy (at least due to deficiency of *Cbs*) is not accompanied by retinal structural/functional changes that differ significantly from age-matched WT littermates. Despite considerable evidence that severe Hhcy is toxic to retina, moderate Hhcy appears tolerated by retina suggesting compensatory cellular survival mechanisms.

Keywords

homocysteine; ganglion cells; cystathionine β-synthase; CBS mouse; retina

1. Introduction

Understanding the basis of retinopathies is critical for developing therapies, especially when mechanistic studies reveal modifiable risk factors. Excess levels of homocysteine (Hcy) have been investigated as possibly causative in several retinal diseases (Ostrakhovitch and Tabibzadeh, 2019; Ajith et al, 2015) including pseudoexfoliation glaucoma (Turgut et al, 2010; Pasquale et al, 2016) and macular degeneration (Huang et al, 2015; Pinna et al, 2018). Its role as a biomarker versus pathogenic factor is unclear. Hcy is a sulfur-containing amino acid positioned at the intersection of the transsulfuration and remethylation metabolic pathways (Fig. 1). It is derived from dietary methionine and converted via the transsulfuration pathway to cystathionine in the presence of vitamin B6, serine and cystathionine beta synthase (CBS) (Sbodio et al, 2019). Cystathionine is an intermediate in the production of cysteine, which is used in production of glutathione, taurine and hydrogen sulfide. Glutathione is a major antioxidant; taurine is an osmoregulatory and immunomodulatory amino acid; and hydrogen sulfide is a gaseous signaling molecule with neuroprotective benefits. Converting Hcy to its downstream products is beneficial; however elevated Hcy, termed hyperhomocysteinemia (Hhcy), has been associated with pathological conditions including neurodegenerative and cardiovascular diseases (Smith et al, 2021). The retina is a neurovascular tissue, thus, it is not surprising that Hhcy has been investigated for its role in retinal diseases. The notion of Hhcy as potentially causative in disease is important because levels of Hcy can be modified by dietary/pharmaceutical supplementation, especially with folate and other B-vitamins. It is not clear, however, if Hhcy has a mechanistic role in retinal diseases.

Some years ago, our laboratory began systematically addressing effects of Hhcy in retina using *in vitro* and *in vivo* models. Our data showed unequivocally that under *in vitro* conditions, Hhcy induces death of retinal ganglion cells (RGCs). For example, at least 50% of freshly isolated mouse primary RGCs die within 18h when cultured in medium containing 50μM Hcy (Dun et al, 2007). Similarly high doses of Hcy induced inflammation in cultured retinal endothelial cells (Elsherbiny et al, 2020). These data must be interpreted cautiously, however, because cell culture conditions are distinct from the intact retinal milieu. In support of this caution is the observation that cultured primary Müller glial cells incubated in medium containing 50μM Hcy actually demonstrated *decreased* oxidative stress and *increased* levels of glutathione (Navneet et al, 2019a). Moreover, when primary RGCs

were indirectly co-cultured with Müller cells in the presence of Hhcy, RGC death was markedly attenuated (Navneet et al, 2019b). The data suggest that not all retinal cell types are adversely affected by Hhcy and that Müller cells may be able to provide significant trophic support to mitigate the short term excitotoxic effects of elevated Hcy exposure. (In these *in vitro* studies, Hcy-thiolactone was administered. Under physiologic conditions, less than 1% of total Hcy is present in a free reduced form. The majority of plasma Hcy (~80%) is *S*- or *N*-homocysteinylated proteins and the precursor of *N*-homocysteinlyated protein is Hcy-thiolactone, a five-membered cyclic thioester (Chubarov, 2021).

The *in vitro* data raise the question as to consequences of Hhcy exposure *in vivo*. Investigations have used two approaches to this question. One involves intravitreal exposure to Hcy (typically as Hcy-thiolactone), which at high concentrations [e.g. 200μM] is acutely toxic to mouse retina (Navneet et al, 2019b; Moore et al, 2001; Chang et al, 2011). The second approach evaluates genetic models of Hhcy, including those with mutations in the Hcy metabolic pathway such as homo- and heterozygosity of *Cbs* (Watanabe et al, 1995). While complete absence of CBS is not compatible with longevity (mice typically die within 3–5 weeks of birth), the heterozygous mice ($Cbs^{+/-}$) live a normal lifespan. The plasma Hcy level in $Cbs^{+/-}$ mice is ~13 nmol/ml, which is twice that of WT mice (~6 nmol/ml). Thus, $Cbs^{+/-}$ mice reflect moderate Hhcy (e.g., in humans, normal plasma Hcy levels are defined as <15μM/L; moderate levels are 15–30μM/L, intermediate levels are 30–100μM/L and severe levels are >100μM/L). In terms of retinal Hcy levels, WT mice have ~0.2 pmol/μg protein and $Cbs^{+/-}$ mice have ~0.4 pmol/μg protein (Ganapathy et al, 2009).

We recently investigated retinal structure and function in $Cbs^{+/-}$ mice at 4, 7 and 10 months (Navneet et al, 2019b). We were anticipating that retinal structure and visual acuity would diminish with age in $Cbs^{+/-}$ mice compared to WT, suggesting a negative impact of chronic, moderate Hhcy on retina. Instead, we found minimal differences in structure or acuity in $Cbs^{+/-}$ mice compared to WT at 4, 7 or 10 months. Indeed, the only significant deficits observed in $Cbs^{+/-}$ mice occurred in a cohort of mice that were deficient in the antioxidant transcription factor NRF2 ($Cbs^{+/-}/Nrf2^{-/-}$). To address the possibility that the previous study evaluating $Cbs^{+/-}$ mice ended prematurely and that a longer period of chronic exposure to moderate Hhcy would result in retinopathy, we designed the current study in which we evaluated comprehensively retinal structure and function in 20 month $Cbs^{+/-}$ mice and compared the findings to age-matched WT mice. Our findings suggest that chronic, moderate Hhcy (at least that which is observed in $Cbs^{+/-}$ mice) is not accompanied by structural or functional changes in the retina that differ significantly from age-matched WT littermates.

2. Methods and materials.

2.1. Animals

Table 1 provides information about the mice used in the study. Breeding pairs of $Cbs^{+/-}$ mice (C57BL/6J-Cbs^{tm1Unc}, stock number 002853; Jackson Laboratories, Bar Harbor, ME, USA) were used to establish our colony of this strain. The *Cbs* deficient mutation was developed in the laboratory of Dr. N. Maeda (University of North Carolina, Chapel Hill, NC) (Watanabe et al, 1995). Age-matched littermates of $Cbs^{+/-}$ and $Cbs^{+/+}$ (WT) were evaluated;

males and females were used in approximately equal numbers. Genotyping was confirmed and representative data are shown (Suppl. Fig. 1). The *Crb1*$^{rd8/rd8}$ mutation associated with focal retinal disruption in some mouse strains (Chang et al, 2013), was not detected in any mice used in the study. Mice were fed Teklad Irradiated Rodent Diet 8904 for breeding or Diet 2918 for maintenance (Teklad, Madison, WI, USA). Animals were subjected to a standard 12-hour light: 12-hour dark cycle. Maintenance and treatment of animals adhered to institutional guidelines for humane treatment of animals and to the ARVO statement for Use of Animals in Ophthalmic and Vision Research.

2.2. Evaluation of intraocular pressure.

Intraocular pressure (IOP) was measured in mice briefly anesthetized using inhaled isofluorane (Butler Animal Health Supply, Dublin, OH, USA). IOP was measured via non-invasive rebound tonometry using a handheld tonometer (Tonolab, Icare Laboratory, Finland) positioned on the cornea. Three repeated measurements were taken from each animal for quantification. Typical IOP measured in normal mice using rebound tonometry is ~10–12 mmHg.

2.3. Evaluation of visual acuity and contrast sensitivity.

To assess visual acuity, spatial thresholds for optomotor tracking of sine-wave gratings were measured using the OptoMotry system (CerebralMechanics, Medicine Hat, Alberta, Canada) as described (Wang et al, 2021; Navneet et al, 2019b). Vertical sine-wave gratings moving at 12°/s or gray of the same mean luminance are projected as a virtual cylinder on four linked computer monitor screens. The unrestrained mouse is perched upon a pedestal in the epicenter of the cylinder. The cylinder hub is continually centered between the mouse's eyes to set the spatial frequency (SF). The SF threshold is measured by systematically increasing the frequency of the grating at 100% contrast until the animal no longer tracks. Grating rotation under these circumstances elicits reflexive optomotor tracking, which is scored via live video using a method of limits procedure with a yes/no criterion. Additionally, the contrast sensitivity function is generated using an adaptation of the aforementioned procedures. The testing at a constant SF of 0.092 cycles/degree begins with a grating of 100% contrast, which is systematically reduced until the contrast threshold is identified. This is the minimum contrast that generates tracking over an SF range between 0.03 and 3.5 cycles/degree and plotted as described (Prusky et al, 2004).

2.4. Evaluation of retinal structure and function

2.4.1 Spectral domain optical coherence tomography (SD-OCT)—Retinal structure was evaluated using SD-OCT as described (Navneet et al, 2019b; Wang et al, 2021). Briefly, mice were anesthetized by intraperitoneal (*i.p.*) injection of ketamine 80mg/kg, xylazine 10mg/kg; retinal architecture was assessed using the Bioptigen SD Ophthalmic Imaging System (Bioptigen Envisu R2200, NC). The imaging protocol included averaged single B scan and volume intensity scans with images centered on the optic nerve head. Post-imaging analysis included autosegmentation analysis and manual assessment of retinal layers using InVivoVue™ Diver 2.4 software (Bioptigen). Measurements included the nerve fiber layer (NFL), inner plexiform layer (IPL), inner nuclear layer (INL), outer

plexiform layer (OPL), and outer nuclear layer + inner segments (ONL+IS), outer segments (OS) and retinal pigment epithelium (RPE). Each layer thickness was plotted separately; data for a given retinal layer in each group were averaged.

2.4.2. Electroretinography (ERG)—Rod and cone function was evaluated in mice anesthetized as described for OCT. ERGs were performed using the Touch/Touch feature of the Celeris Ophthalmic Electrophysiology System (Diagnosys, Lowell, MA) as described (Wang et al, 2021). Corneal moisture was maintained using 0.3% hypromellose solution. Mice, dark-adapted overnight prior to scotopic ERGs, were tested using a series of increasing light flashes intensities (0.001, 0.005, 0.01, 0.1, 0.5, and 1.0 cd.s/m^2). Light-adapted (photopic) testing was initiated during which time rods were saturated using the adaptive light background feature of the Celeris system. The light adaptation time for the Celeris system is typically 2–5 min; here, we used 5 minutes. Photopic testing was performed using flashes of 3, 10, 25, 50, 100, and 150 cd.s/m^2.

2.4.3. Pattern ERG (pERG)—pERG was performed to assess RGC function in dark adapted mice. Just prior to the procedure, mice were anesthetized as described for OCT. Pupils were dilated maximally with 0.5% tropicamide and 2.5% phenylephrine eye drops. Mice were placed on a heated platform (37°C). The pattern stimulator was placed in contact with the eye; the flash stimulator for the contralateral eye acted as the reference electrode. Transient pERG responses were recorded using black and white horizontal bar stimuli delivered using the Celeris system per the manufacturer's guidelines. The parameters for pERG amplitude were spatial frequency 0.125 cycles/degree, a luminance of 50 cd.s/m^2, contrast 100% and substantial averaging (600 sweeps). The data were analyzed by the software Espion V6 (Diagnosys). The P1-N2 amplitude, measured from the P1 peak to the nadir of N2, was used to analyze the RGC function.

2.5. Morphometric and immunohistochemical analyses of retinas.

Eyes were either immersion fixed in 2% paraformaldehyde/2% glutaraldehyde in 0.1M cacodylate buffer and processed for embedding in JB-4 methacrylate (Electron Microscopy Sciences, Hatfield, PA) for morphometry or were flash frozen in liquid nitrogen and embedded in optimal cutting temperature compound (Elkhart, IN) for immunohistochemistry. For morphometry, JB-4-embedded eyes were stained with hematoxylin and eosin (H&E) and were visualized at low magnification for evidence of gross disruption and imaged at higher magnification using a Zeiss Axio Imager D2 microscope (Carl Zeiss, Göttingen, Germany) equipped with a high-resolution camera. Retinas were subjected to systematic measurement of total thickness and the thickness of the individual retinal layers using Zeiss Zen23pro software. Measurements were taken at six points along the retina, three adjacent fields on the temporal and nasal sides beginning 200μm from the optic nerve. The measurements were averaged per eye per group and expressed as mean ± standard error of the mean (SEM).

For immunohistochemistry, 10μm thick cryosections were fixed 10 min in 4% paraformaldehyde, blocked with Powerblock (BioGenex, Fremont, CA) for 1h at room temperature. Sections were incubated with anti-goat Brn3a antibody (SC31984, Santa

Cruz Corp., Santa Cruz, CA) at a dilution of 1:200 and detected using Alexa Fluor 488 anti-Goat IgG (H + L) Invitrogen Molecular Probes, NY (1:1000). Brn3a is a marker for RGCs (Nadal-Nicolás et al, 2009). To quantify the number of Brn3a-positive cells, retinal sections were imaged using the 20X objective of the microscope. Per mouse, six regions of retina were evaluated, 3 on the nasal and 3 on the temporal side of the optic nerve. The number of RGCs/retinal section was expressed per 100μm retinal length. The data were averaged per mouse. To detect oxidative stress, dyhydroethidium (also called hydroethidine) (D11347; Molecular Probes-Thermofisher) was used in retinal cryosections following our protocol (Wang et al, 2016). Dydroethidium (DHE) is an indicator of superoxide levels, which typically exhibits a blue-fluorescence in the cytosol until oxidized, in which case it intercalates with DNA, staining the cell nucleus a bright fluorescent red. The average fluorescent intensity of DHE was recorded for each section evaluated and the data were averaged per mouse. To detect gliosis in retinas, glial fibrillary acid protein (GFAP) was analyzed. Sections were incubated with rabbit anti-GFAP (Z0334, Dako, Carpentaria, CA) at a dilution of 1:500 and detected using Alexa Fluor 488 anti-Rabbit IgG (H + L) Invitrogen (Molecular Probes-Thermofisher) at a dilution of 1:1000. Omission of the secondary antibody served as a negative control. Fluorescent intensity of GFAP was recorded per section and averaged per mouse. Retinal cryosections were viewed by immunofluorescence using the Zeiss Axio Imager D2 microscope.

2.6 Data analysis

Data analysis utilized GraphPad Prism 9 for Windows Version 9.2.0 statistical analysis software (GraphPad, La Jolla, CA). Data were analyzed by one- or two-way ANOVA as appropriate; in cases of significance Tukey's Multiple Comparisons test was the post-hoc test. All values are reported as mean ± SEM. For all analyses $p < .05$ was considered statistically significant.

3. Results

3.1. Assessment of intraocular pressure (IOP)

IOP was evaluated in *Cbs*$^{+/-}$ and WT mice. The pressure averaged 10 mmHg for mice at 12 and 20 months, regardless whether they had excess Hcy or not (Suppl. Fig. 2). Increasing age does not appear to be associated with increased IOP in mice with moderate Hhcy due to deficiency of CBS.

3.2. Assessment of visual acuity, contrast sensitivity and retinal architecture in vivo

Visual acuity and contrast sensitivity were measured using the OptoMotry system. Earlier studies in 10–11 month *Cbs*$^{+/-}$ mice showed an average response of ~0.38 cycles/degree (c/d), which did not differ significantly from age-matched WT mice (Navneet et al, 2019b). Here, we confirmed that the visual acuity in 12 month *Cbs*$^{+/-}$ mice was similar to WT (~0.38 c/d) (Fig. 2A). In the 20 month old animals there was a slight decrease in acuity (~0.35 – 0.36 c/d), however there was no significant difference between age-matched *Cbs*$^{+/-}$ and WT mice. There was also no difference in the contrast sensitivity measured in *Cbs*$^{+/-}$ mice versus WT at either 12 or 20 months (Fig. 2B).

Retinal architecture was evaluated using SD-OCT in *Cbs*$^{+/-}$ mice that were 20 months of age compared to age-matched WT mice. Volume intensity projections and OCT B-scans (Fig. 2C) were analyzed and layer thicknesses quantified using DIVERS software. This program allows systematic morphometric analysis of each of the retinal layers and measurements can be made in the same plane (e.g. nasal-temporal) to permit comparison. There was no significant difference in the total retinal thickness between 20 month *Cbs*$^{+/-}$ mice and 20 month WT mice, nor were there significant differences for the other retinal layers including the NFL, IPL or ONL (Fig. 2D).

3.3. Assessment of rod, cone and ganglion cell function

Cbs$^{+/-}$ mice were subjected to ERG analysis at 12 and 20 months of age to evaluate rod (scotopic) and cone (photopic) function compared to age-matched WT mice. Representative tracings of rod activity at increasing light intensity are shown for 12 month *Cbs*$^{+/-}$ and WT mice (Suppl. Fig. 3A). The tracings are virtually identical for the two groups. Average scotopic a-wave and b-wave amplitudes are shown (Suppl. Figs. 3B and 3C). The b-wave amplitudes ranged from ~150 – 400μV at the highest light intensity (1.0 cd.s/m^2); there were no differences in the range of scotopic responses (nor the average response) between mutant and WT mice at 12 months. Similarly, representative tracings of cone activity at increasing light levels are shown for *Cbs*$^{+/-}$ and WT mice (Suppl. Fig. 3D). The tracings are similar between the two groups and are robust. The average photopic a- and b-wave amplitudes are shown (Suppl. Figs. 3E and 3F). The photopic b-wave amplitude ranged from 60–125μV and an average of ~75 μV for both *Cbs*$^{+/-}$ and WT mice (Suppl. Fig. 3F). There was no significant difference in photopic responses in 12 month *Cbs*$^{+/-}$ versus WT mice.

In the older mice (20 months), rod responses were generally lower than at 12 months. Representative tracings of rod activity for *Cbs*$^{+/-}$ and WT mice were similar (Fig. 3A). Average scotopic a-wave and b-wave amplitudes are shown for 20 month mice (Fig. 3B, Fig. 3C). The a-waves tend to be erratic at the lowest light flash intensities (0.001, 0.005, 0.01cd) with amplitudes less than 25μV, however at higher flash intensities (0.1cd.s/m^2 and greater), responses were robust in both groups. The b-wave amplitudes ranged from ~50 – 200μV at the highest light intensity (1.0 cd.s/m^2). There were no differences in the range of scotopic responses (nor the average response) between mutant and WT mice. This trend persisted with the analysis of cone function. That is, photopic tracings were similar between *Cbs*$^{+/-}$ and WT mice (Fig. 3D). The average photopic a- and b-wave amplitudes had similar ranges for the two groups (Fig. 3E, Fig. 3F). For example, the photopic b-wave amplitude for 20 month WT mice was ~60μV at a flash intensity of 150 cd.s/m^2, which was the same as the *Cbs*$^{+/-}$ mice (Fig. 3F). Taken collectively, despite prolonged (20 months) exposure to moderate levels of Hcy, the *Cbs*$^{+/-}$ mice had electrophysiologic responses that did not differ significantly from age-matched WT.

RGC function was assessed by measuring pERG responses. P1 and N2 waves of the mouse pattern ERG are dominated by RGC contributions from the ON and OFF pathways, respectively (Miura et al, 2009). Representative pERG tracings are shown for *Cbs*$^{+/-}$ and WT mice at 12 months (Suppl. Fig. 4A) and 20 months (Suppl. Fig. 4B). At 12 months, the average P1-N2 amplitude in both groups of mice was 9–10μV. There was no significant

difference in responses between the groups, although there was a substantial range in responses in both groups (Suppl. Fig. 4C). In the 20 month group, the average P1-N2 amplitude had declined with age and was 6–7μV; there was no difference between *Cbs*$^{+/-}$ and WT mice (Suppl. Fig. 4C). The data suggest that with age, RGC function diminishes in the murine models investigated, however prolonged, moderate Hhcy, due to CBS deficiency, does not compromise RGC function beyond that observed with advanced age.

3.4. Morphometric and immunohistochemical assessment

At the conclusion of *in vivo* functional assessments, 20 month WT and *Cbs*$^{+/-}$ mice were euthanized and eyes harvested for morphometry and immunohistochemistry. Morphometric assessment was performed in eyes embedded in JB-4 methacrylate. Representative retinal images are shown for *Cbs*$^{+/-}$ and WT mice (Fig. 5A, 5B). The general appearance of the retinas of *Cbs*$^{+/-}$ mice is similar to that of age-matched WT, with clear delineation of the retinal nuclear and plexiform layers. Systematic measurement of the total retinal thickness and the thickness of each individual layer revealed no statistical difference between *Cbs*$^{+/-}$ and WT mice (Fig. 5C).

Given that Hhcy is implicated in glaucoma, which affects RGCs, we counted these cells in retinas of 20 month *Cbs*$^{+/-}$ mice compared to WT. Earlier studies of younger *Cbs*$^{+/-}$ mice reported fewer cells in the ganglion cell layer (GCL) compared to age-matched WT mice (Ganapathy et al, 2009; Navneet et al, 2019b), however it was not known whether this difference would persist with advanced age. Here, immunohistochemical methods were used to detect Brn3a, a ganglion cell specific marker. Representative images show intense green fluorescence in the GCL of *Cbs*$^{+/-}$ and WT mice (Fig. 5A). Given that there are two neuronal cell types in the GCL (ganglion and amacrine), we counted the number of Brn3a-positive cells and Brn3a-plus-DAPI-labeled cells. There were typically ~5 Brn3a-positive cells and approximately 10 cells total per 100μm retinal length. There was no difference in the number of cells or specifically Brn3a-positive cells in 20 month *Cbs*$^{+/-}$ mice compared to age-matched WT (Fig. 5B). As anticipated, there were more Brn3a-positive cells in young WT mice (age: 4 months) compared to the 20 month mice (Fig. 5B).

We asked whether oxidative stress was a feature of retinas at 20 months and whether there was a difference between *Cbs*$^{+/-}$ mice compared to WT by subjecting retinal cryosections to immunolabeling with DHE, which detects superoxide. A representative retinal section from a 4 month WT mouse (used as a ‘young’ control) is shown (Fig. 5C) and there was minimal labeling of DHE at this age. For the 20 month mice, there was modest increased red immunofluorescence, indicative of increased oxidative stress, in both *Cbs*$^{+/-}$ and WT mice. This modest elevation was observed not only in the GCL, but also in the INL and ONL. Quantification of the immunofluorescent intensity revealed a significant increase in the 20 month old retinas compared to the 4 month WT, however there was no difference in intensity between the 20 month *Cbs*$^{+/-}$ and WT mice (Fig. 5D).

We investigated whether there was an increase in gliosis in *Cbs*$^{+/-}$ mice compared to age-matched WT mice. Gliosis was detected by immunolabeling for GFAP. GFAP expression is limited in the healthy retina, but in the presence of retinal pathology, Müller cells upregulate GFAP and a radial pattern of labeling is observed (Reichenbach and Bringmann, 2013). In

earlier studies of *Cbs*$^{+/-}$ mice (at 10–11 months), GFAP labeling was minimal. In the present work, we evaluated levels of GFAP in 20 month *Cbs*$^{+/-}$ and WT mice and compared findings to young (4 month WT mice) (Fig. 5E). There was minimal labeling of retinas of young mice, but a notable increase in the 20 month *Cbs*$^{+/-}$ mice. Quantification of fluorescence intensity revealed a significant difference between retinas of young mice compared to the older mice, but no significant difference between the 20 month *Cbs*$^{+/-}$ and WT mice (Fig. 5F).

4. Discussion

The present work was prompted by studies in human patients in which Hhcy was evaluated as potentially pathogenic in retinal diseases such as glaucoma and age-related macular degeneration (Ostrakhovitch and Tabibzadeh, 2019; Ajith and Ranimenon, 2015; Turgut et al, 2010; Clement et al, 2009; Aboobakar et al, 2017; Ritch, 1994; Huang et al, 2015; Pinna et al, 2018). There are conflicting data in human glaucoma patients (Pasquale et al, 2016, Lin et al, 2020) and macular degeneration patients (Christen et al, 2015; Christen et al, 2018) as to the validity of this claim. To address this, basic research studies have used cell culture models, intravitreal injection of high dosages of Hcy (particularly Hcy-thiolactone), and genetic models with mutations in the Hcy metabolic pathway. Cell culture and intravitreal injection models provide convincing data that high levels of Hcy are toxic to retinal cells (Dun et al, 2007; Elsherbiny et al, 2020). These two experimental systems do not mimic the more common *in vivo* exposure to Hhcy, which in the general population is fortunately moderate (15–30μM) to intermediate (30–100μM), rather than severe (>100μM), compared to normal levels <15μM. The prevalence of Hhcy is between 10–30% of the population, but may be higher in the elderly (Selhub, 2008), thus examining the effects of Hhcy as a function of aging is relevant. The mouse heterozygous for mutation of *Cbs*$^{+/-}$ used in this study has plasma and retinal Hcy levels that are ~twice normal (Watanabe et al, 1995; Ganapathy et al, 2009), thus they serve as a useful tool to assess short- and long-term consequences of chronic exposure to retina to moderate Hhcy.

Previous *in vivo* studies performed in our laboratory of young *Cbs*$^{+/-}$ mice showed minimal disruption of the retina and equivalent numbers of cells in the GCL between mutant mice and age-matched WT littermates (Ganapathy et al, 2009). Subsequent studies of older *Cbs*$^{+/-}$ mice (10 months) revealed significantly fewer cells in the GCL of mutants compared to controls, although the mild loss of cells did not translate to diminished visual acuity as measured by the OMR response (Navneet et al, 2019b). We found this intriguing and questioned whether the study had ended prematurely. That is, perhaps the endpoint of 10 months may not have allowed sufficient time for the impact of moderate Hhcy on visual acuity, structure and function to be fully observed.

Therefore, we undertook the present experiment in which we analyzed retinal function and structure comprehensively in *Cbs*$^{+/-}$ mice at 20 months of age. To summarize, IOP levels were well within normal limits. Visual acuity did not differ between *Cbs*$^{+/-}$ and WT mice. SD-OCT analyses revealed well organized retinal layers with no evidence of disruption in inner or outer retina. It is noteworthy, that in one study evaluating *Cbs*$^{+/-}$ mice, focal disruptions of the outer retina were reported in OCT studies of *Cbs*$^{+/-}$ mice at 24 weeks

(Ibrahim et al, 2016) [see figure 1], but the phenotype is reminiscent of the disruption observed in the *Rd8* mutation of the *Crb1* gene, which has been reported in some vendor lines (Mattapallil et al, 2012) [see figure 2]. The current analysis of 20 month $Cbs^{+/-}$ mice, which do not harbor the *Rd8* mutation, suggests that chronic exposure to mild-moderate Hhcy does not result in long-term pathology and that the *in vivo* retinal architecture is quite similar to age-matched WT littermates.

There have been a few studies of electrophysiological responses in $Cbs^{+/-}$ mice. A study conducted over an age range of 5 – 30 weeks showed a mild decrease of the a- and b-wave amplitudes in $Cbs^{+/-}$ mice compared to WT (Yu et al, 2012). The current study of 20 month $Cbs^{+/-}$ mice showed no significant differences in scotopic or photopic ERG responses compared to age-matched WT littermates. Evaluation specifically of RGC function using pERG also showed no significant difference by 20 months in the $Cbs^{+/-}$ mice versus WT. Thus, our data suggest that by 20 months, any differences in rod, cone or RGC function that might have emerged as a function of increased Hcy levels at younger ages were no longer appreciable when mice were nearly 2 years old. Similarly, histological analysis of retinas of $Cbs^{+/-}$ mice revealed normal appearance with no disruption of inner or outer retina including outer segments/RPE. The number of RGCs was similar between $Cbs^{+/-}$ mice and age-matched WT mice. Oxidative stress and gliosis were significantly less in young (4 month) WT mice than 20 month mice, but did not differ between $Cbs^{+/-}$ and WT.

The present study is important because assumptions have been made about the role of Hhcy in the pathogenesis of retinal diseases, particularly glaucoma and age-related macular degeneration. Regarding glaucoma, there have definitely been reports of severely elevated Hcy and glaucoma. Notably a recent report of a 14-year old male with glaucoma and lens dislocation indicated Hcy levels that were 20 fold greater than normal (>300μM/L) (Hua et al, 2021). The youngster was treated with pyridoxine (vitamin B6), a low-methionine diet, and anti-glaucoma eye drops (carteolol hydrochloride 2% and brinzolamide 1%). The glaucoma, characterized by an IOP of 45mmHg, was due to displacement of the lens to the anterior chamber. The treatment plan yielded improvement in Hcy levels and reduced IOP. This scenario is a case of excessively high levels of Hcy leading to serious visual problems. The cause of the Hhcy involved two separate mutations in the *CBS* gene, although the patient's parents each had a single *CBS* genetic mutation and both had normal vision. Far more prevalent are studies of adults with glaucoma (pseudoexfoliation glaucoma, primary open angle glaucoma etc) and associated plasma Hcy levels (Aboobakar et al, 2017). Some studies suggest a relationship between various forms of glaucoma and elevated plasma Hcy (Koc and Kaya, 2020; Lin et al, 2020; Lee et al, 2017, Rebecca et al, 2019). Other studies suggest that there is, at best, a tenuous relationship between the two (Pasquale et al, 2016; Zheng et al, 2020). Indeed, at the 21st annual meeting of The Glaucoma Foundation Think Tank (2014), attendees concluded that it was not clear how mild Hhcy (as seen in pseudoexfoliation glaucoma) could contribute to disarrayed extracellular aggregates characteristic of this syndrome (Pasquale et al, 2016). The conference discussion instead emphasized the relevance of mutations in *LOXL1* and *CACNA1A* as risk factors for the disease.

Regarding age-related macular degeneration, there have been a number of studies that suggest a positive correlation in disease manifestation with increasing levels of Hhcy (Ostrakhovitch and Tabibzadeh, 2019; Ajith and Ranimenon, 2015). However, data from large population studies (evaluating more than 25,000 patients) do not support this correlation (Christen et al, 2015; Christen et al, 2018). The data obtained in the current study do not reflect disruption of the photoreceptor cell layer, the inner/outer segments or the RPE.

The findings of the present study of *Cbs*$^{+/-}$ mice suggest limited long-term impact of moderate Hhcy on retinal function and structure *in vivo* and *in situ*, when corrected for age. Our group has studied the *Cbs*$^{+/-}$ mouse model for a number of years (Ganapathy et al, 2009; Yu et al, 2012; Ganapathy et al, 2011a; Ganapathy et al, 2011b; Tawfik et al, 2014). We know from previous studies that during the first few months of life, there is a significant difference between the number of RGCs and the thickness of the NFL in the mutant versus age-matched controls, although little effect on IOP (Navneet et al, 2019b). It appears, however, that with advancing age the differences observed in *Cbs*$^{+/-}$ mice versus age-matched controls decrease. It may be that compensatory mechanisms in the *Cbs*$^{+/-}$ retina attenuate cellular loss and functional deficits. We speculate on two possibilities regarding the apparent compensation for moderate Hhcy. One possibility is that supportive cells, such as Müller glia, are activated over the course of the chronic exposure and buffer moderate Hcy elevations such that the retinal neurons are spared an excessively excitotoxic milieu. Evidence for this theory comes from work using an indirect co-culture model in which primary Müller cells mitigated death of primary RGCs that had been exposed to high levels of Hcy-thiolactone (Navneet et al, 2019b). It is known that excess Hcy-thiolactone levels impair RGC mitochondrial dynamics (Ganapathy et al, 2011a). Interestingly, however, studies of Müller cells showed that excess Hcy-thiolactone did not impair mitochondrial function. Instead, Müller cells had higher spare respiratory capacity compared to non-treated control cells (Navneet et al, 2019b). Spare respiratory capacity is indicative of the cells' capacity to respond to energetic demands. Thus, Müller cells have a robust capacity to respond to the demands of the excitotoxic stress induced by Hhcy, at least under *in vitro* circumstances. Indeed, excess Hcy-thiolactone has been shown to increase expression of the NRF2 antioxidant pathway (Navneet et al, 2019a). Whether this accounts for the mild response to Hhcy in the *Cbs*$^{+/-}$ mice and the apparent ability of the retina to buffer exposure to this excitotoxin remains to be determined.

Another potential explanation for the apparent capacity to buffer Hhcy in the *Cbs*$^{+/-}$ retina is the report that levels of OPA1 (optic atrophy 1 protein) are actually increased in the mutant compared to WT (Ganapathy et al, 2011a). OPA1 is an inner mitochondrial membrane remodeling protein that is essential for RGC health. Mutations in the gene encoding this protein cause hereditary optic neuropathy via mitochondrial dysfunction (Delettre et al, 2000). Interestingly, not only is OPA1 increased in the *Cbs*$^{+/-}$ retina, but the S-OPA1 form, which appears to support cellular survival in stress (Lee and Yoon, 2016; Lee et al, 2017), is also increased in this mutant (Ganapathy et al, 2011a). A future direction of the present study will be to investigate potential mechanisms by which RGCs, and other retinal neurons, manage to survive under Hhcy conditions.

Hhcy is not only implicated in neurodegenerative diseases, but it has also been evaluated as causative in vascular diseases in patients including cardiovascular, cerebrovascular and thromboembolic diseases (Chrysant and Chrysant, 2018; Koklesova et al, 2021). Thus, related to the current work, which focused on evaluation of retinal neuronal function in *Cbs*$^{+/-}$ mice of advanced age, another area of investigation could be analyses of retinal vasculature in aging *Cbs*$^{+/-}$ mice. We have conducted retinal vascular analyses in younger *Cbs*$^{+/-}$ mice and observed differences between WT and mutant mice (Tawfik et al, 2013; Tawfik et al, 2014), however whether this persists in older mice remains to be investigated.

Supplementary Material

Refer to Web version on PubMed Central for supplementary material.

Acknowledgements

This work was supported by the National Eye Institute/NIH (R01 EY012830, R01 EY028103, R21 EY031483, P30 EY031631). We thank Donna Kumiski and Tania Green for excellent assistance with histologic processing of tissue for light microscopic and immunohistochemical studies.

References

Aboobakar IF, Johnson WM, Stamer WD, Hauser MA, Allingham RR 2017. Major review: Exfoliation syndrome; advances in disease genetics, molecular biology, and epidemiology. Exp Eye Res. 154:88–103. [PubMed: 27845061]

Ajith TA, Ranimenon. 2015. Homocysteine in ocular diseases. Clin Chim Acta. 450:316–21. [PubMed: 26343924]

Chang B, Hurd R, Wang J, Nishina P 2013. Survey of common eye diseases in laboratory mouse strains. Invest Ophthalmol Vis Sci. 54:4974–81. [PubMed: 23800770]

Chang HH, Lin DP, Chen YS, Liu HJ, Lin W, Tsao ZJ, Teng MC, Chen BY 2011 Intravitreal homocysteine-thiolactone injection leads to the degeneration of multiple retinal cells, including photoreceptors. Mol Vis. 17:1946–56. [PubMed: 21850169]

Christen WG, Cook NR, Chiuve SE, Ridker PM, Gaziano JM 2018. Prospective study of plasma homocysteine, its dietary determinants, and risk of age-related macular degeneration in men. Ophthalmic Epidemiol. Ophthalmic epidemiology. 25:79–88.

Christen WG, Cook NR, Ridker PM, Buring JE 2015. Prospective study of plasma homocysteine level and risk of age-related macular degeneration in women. Ophthalmic epidemiology. 22:85–93. [PubMed: 25777307]

Chrysant SG, Chrysant GS 2018. The current status of homocysteine as a risk factor for cardiovascular disease: a mini review. Expert Rev Cardiovasc Ther. 16:559–65. [PubMed: 29979619]

Chubarov AS 2021. Homocysteine Thiolactone: Biology and Chemistry. Encyclopedia 1: 445–59.

Clement CI, Goldberg I, Healey PR, Graham SL 2009. Plasma homocysteine, MTHFR gene mutation, and open-angle glaucoma. J Glaucoma. 18:73–8. [PubMed: 19142139]

Delettre C, Lenaers G, Griffoin JM, Gigarel N, Lorenzo C, Belenguer P, Pelloquin L, Grosgeorge J, Turc-Carel C, Perret E, Astarie-Dequeker C, Lasquellec L, Arnaud B, Ducommun B, Kaplan J, Hamel CP. 2000. Nuclear gene OPA1, encoding a mitochondrial dynamin-related protein, is mutated in dominant optic atrophy. Nat Genet. 26:207–10. [PubMed: 11017079]

Dun Y, Thangaraju M, Prasad P, Ganapathy V, Smith SB 2007. Prevention of excitotoxicity in primary retinal ganglion cells by (+)-pentazocine, a sigma receptor-1 specific ligand. Invest Ophthalmol Vis Sci. 48:4785–94. [PubMed: 17898305]

Elsherbiny NM, Sharma I, Kira D, Alhusban S, Samra YA, Jadeja R, Martin P, Al-Shabrawey M, Tawfik A 2020. Homocysteine Induces Inflammation in Retina and Brain. Biomolecules. 10:393.

Ganapathy PS, Moister B, Roon P, Mysona BA, Duplantier J, Dun Y, Moister TK, Farley MJ, Prasad PD, Liu K, Smith SB 2009. Endogenous elevation of homocysteine induces retinal neuron death in the cystathionine-beta-synthase mutant mouse. Invest Ophthalmol Vis Sci. 50:4460–70. [PubMed: 19357353]

Ganapathy PS, Perry RL, Tawfik A, Smith RM, Perry E, Roon P, Bozard BR, Ha Y, Smith SB 2011a. Homocysteine-mediated modulation of mitochondrial dynamics in retinal ganglion cells. Invest Ophthalmol Vis Sci. 52:5551–8. [PubMed: 21642619]

Ganapathy PS, White RE, Ha Y, Bozard BR, McNeil PL, Caldwell RW, Kumar S, Black SM, Smith SB 2011b. The role of N-methyl-D-aspartate receptor activation in homocysteine-induced death of retinal ganglion cells. Invest Ophthalmol Vis Sci. 52:5515–24. [PubMed: 21436276]

Hua N, Ning Y, Zheng H, Zhao L, Qian X, Wormington C, Wang J 2021. Recurrent dislocation of binocular crystal lenses in a patient with cystathionine beta-synthase deficiency. BMC Ophthalmol. 21:212. [PubMed: 33985475]

Huang P, Wang F, Sah BK, Jiang J, Ni Z, Wang J, Sun X 2015. Homocysteine and the risk of age-related macular degeneration: a systematic review and meta-analysis. Sci Rep. 21;5:10585. [PubMed: 26194346]

Ibrahim AS, Mander S, Hussein KA, Elsherbiny NM, Smith SB, Al-Shabrawey M, Tawfik A 2016.Hyperhomocysteinemia disrupts retinal pigment epithelial structure and function with features of age-related macular degeneration. Oncotarget. 7:8532–45. [PubMed: 26885895]

Koc H, Kaya F 2020. Relationship between homocysteine levels, anterior chamber depth, and pseudoexfoliation glaucoma in patients with pseudoexfoliation. Int Ophthalmol. 40:1731–1737. [PubMed: 32212027]

Koklesova L, Mazurakova A, Samec M, Biringer K, Samuel SM, Büsselberg D, Kubatka P, Golubnitschaja O 2021. Homocysteine metabolism as the target for predictive medical approach, disease prevention, prognosis, and treatments tailored to the person. EPMA J. 11:1–29.

Lee H, Smith SB, Yoon Y 2017. The short variant of the mitochondrial dynamin OPA1 maintains mitochondrial energetics and cristae structure. J Biol Chem. 292:7115–7130. [PubMed: 28298442]

Lee H, Yoon Y 2016. Mitochondrial fission and fusion. Biochem Soc Trans. 44:1725–1735. [PubMed: 27913683]

Lee JY, Kim JM, Kim IT, Yoo CK, Won YS, Kim JH, Kwon HS, Park KH 2017. Relationship between Plasma Homocysteine Level and Glaucomatous Retinal Nerve Fiber Layer Defect. Curr Eye Res. 42:918–923. [PubMed: 28094585]

Lin Z, Huang S, Yu H, Sun J, Huang P, Zhong Y 2020. Analysis of Plasma Hydrogen Sulfide, Homocysteine, and L-Cysteine in Open-Angle Glaucoma Patients. J Ocul Pharmacol Ther. 36:649–657. [PubMed: 32493106]

Markand S, Saul A, Roon P, Prasad P, Martin P, Rozen R, Ganapathy V, Smith SB 2015. Retinal Ganglion Cell Loss and Mild Vasculopathy in Methylene Tetrahydrofolate Reductase (Mthfr)-Deficient Mice: A Model of Mild Hyperhomocysteinemia. Invest Ophthalmol Vis Sci. 56:2684–95. [PubMed: 25766590]

Mattapallil MJ, Wawrousek EF, Chan CC, Zhao H, Roychoudhury J, Ferguson TA, Caspi RR 2012. The Rd8 mutation of the Crb1 gene is present in vendor lines of C57BL/6N mice and embryonic stem cells, and confounds ocular induced mutant phenotypes. Invest Ophthalmol Vis Sci. 53:2921–7. [PubMed: 22447858]

Miura G, Wang MH, Ivers KM, Frishman LJ 2009. Retinal pathway origins of the pattern ERG of the mouse. Exp. Eye Res. 89:49–62. [PubMed: 19250935]

Moore P, El-sherbeny A, Roon P, Schoenlein PV, Ganapathy V, Smith SB 2001. Apoptotic cell death in the mouse retinal ganglion cell layer is induced in vivo by the excitatory amino acid homocysteine. Exp Eye Res. 73:45–57. [PubMed: 11428862]

Nadal-Nicolás FM, Jiménez-López M, Sobrado-Calvo P, Nieto-López L, Cánovas-Martínez I, Salinas-Navarro M, Vidal-Sanz M, Agudo M 2009. Brn3a as a marker of retinal ganglion cells: qualitative and quantitative time course studies in naive and optic nerve-injured retinas. Invest Ophthalmol Vis Sci. 50:3860–8. [PubMed: 19264888]

Navneet S, Cui X, Zhao J, Wang J, Kaidery NA, Thomas B, Bollinger KE, Yoon Y, Smith SB 2019a. Excess homocysteine upregulates the NRF2-antioxidant pathway in retinal Müller glial cells. Exp Eye Res. 178:228–237. [PubMed: 29608906]

Navneet S, Zhao J, Wang J, Mysona B, Barwick S, Ammal Kaidery N, Saul A, Kaddour-Djebbar I, Bollag WB, Thomas B, Bollinger KE, Smith SB 2019b. Hyerhomocysteinemia-induced death of retinal ganglion cells: The role of Müller glial cells and NRF2. Redox Biol. 24:101199. [PubMed: 31026769]

Ostrakhovitch EA, Tabibzadeh S 2019. Homocysteine and age-associated disorders. Ageing Res Rev. 49:144–164. [PubMed: 30391754]

Pasquale LR, Borrás T, Fingert JH, Wiggs JL, Ritch R 2016. Exfoliation syndrome: assembling the puzzle pieces. Acta Ophthalmol. 94:e505–12. [PubMed: 26648185]

Pinna A, Zaccheddu F, Boscia F, Carru C, Solinas G 2018. Homocysteine and risk of age-related macular degeneration: a systematic review and meta-analysis. Acta Ophthalmol. 96:e269–e276. [PubMed: 27966830]

Prusky GT, Alam NM, Beekman S, Douglas RM 2004. Rapid quantification of adult and developing mouse spatial vision using a virtual optomotor system. Invest Ophthalmol Vis Sci. 45:4611–6. [PubMed: 15557474]

Rebecca M, Gayathri R, Bhuvanasundar R, Sripriya K, Shantha B, Angayarkanni N 2019. Elastin modulation and modification by homocysteine: a key factor in the pathogenesis of Pseudoexfoliation syndrome? Br J Ophthalmol. 103:985–992. [PubMed: 30249767]

Reichenbach A, Bringmann A 2013. New functions of Müller cells. Glia. 61:651–78. [PubMed: 23440929]

Ritch R 1994. Exfoliation syndrome-the most common identifiable cause of open-angle glaucoma. J Glaucoma. 3:176–7. [PubMed: 19920577]

Sbodio JI, Snyder SH, Paul BD 2019. Regulators of the transsulfuration pathway. Br J Pharmacol. 176:583–593. [PubMed: 30007014]

Selhub J 2008. Public health significance of elevated homocysteine. Food Nutr Bull. 29:S116–25. [PubMed: 18709886]

Smith AD, Refsum H 2021. Homocysteine - from disease biomarker to disease prevention. J Intern Med. 290:836–854.

Tawfik A, Al-Shabrawey M, Roon P, Sonne S, Covar JA, Matragoon S, Ganapathy PS, Atherton SS, El-Remessy A, Ganapathy V, Smith SB 2013. Alterations of retinal vasculature in cystathionine-Beta-synthase mutant mice, a model of hyperhomocysteinemia. Invest Ophthalmol Vis Sci. 54:939–49. [PubMed: 23307965]

Tawfik A, Markand S, Al-Shabrawey M, Mayo JN, Reynolds J, Bearden SE, Ganapathy V, Smith SB 2014. Alterations of retinal vasculature in cystathionine-β-synthase heterozygous mice: a model of mild to moderate hyperhomocysteinemia. Am J Pathol. 184:2573–85. [PubMed: 25016930]

Turgut B, Kaya M, Arslan S, Demir T, Güler M, Kaya MK 2010. Levels of circulating homocysteine, vitamin B6, vitamin B12, and folate in different types of open-angle glaucoma. Clin Interv Aging. 5:133–9. [PubMed: 20458351]

Wang J, Saul A, Roon P, Smith SB 2016. Activation of the molecular chaperone, sigma 1 receptor, preserves cone function in a murine model of inherited retinal degeneration. Proc Natl Acad Sci U S A. 113:E3764–72. [PubMed: 27298364]

Wang J, Xiao H, Barwick S, Liu Y, Smith SB 2021. Optimal timing for activation of sigma 1 receptor in the Pde6brd10/J (rd10) mouse model of retinitis pigmentosa. Exp Eye Res. 202:108397. [PubMed: 33310057]

Watanabe M, Osada J, Aratani Y, Kluckman K, Reddick R, Malinow MR, Maeda N 1995. Mice deficient in cystathionine beta-synthase: animal models for mild and severe homocyst(e)inemia. Proc Natl Acad Sci U S A. 92:1585–9. [PubMed: 7878023]

Yu M, Sturgill-Short G, Ganapathy P, Tawfik A, Peachey NS, Smith SB 2012. Age-related changes in visual function in cystathionine-beta-synthase mutant mice, a model of hyperhomocystein-emia. Exp Eye Res. 96:124–31. [PubMed: 22197750]

Zheng M, Zheng Y, Gao M, Ma H, Zhang X, Li Y, Wang F, Huang H 2020. Expression and clinical value of lncRNA MALAT1 and lncRNA ANRIL in glaucoma patients. Exp Ther Med. 19:1329–1335. [PubMed: 32010306]

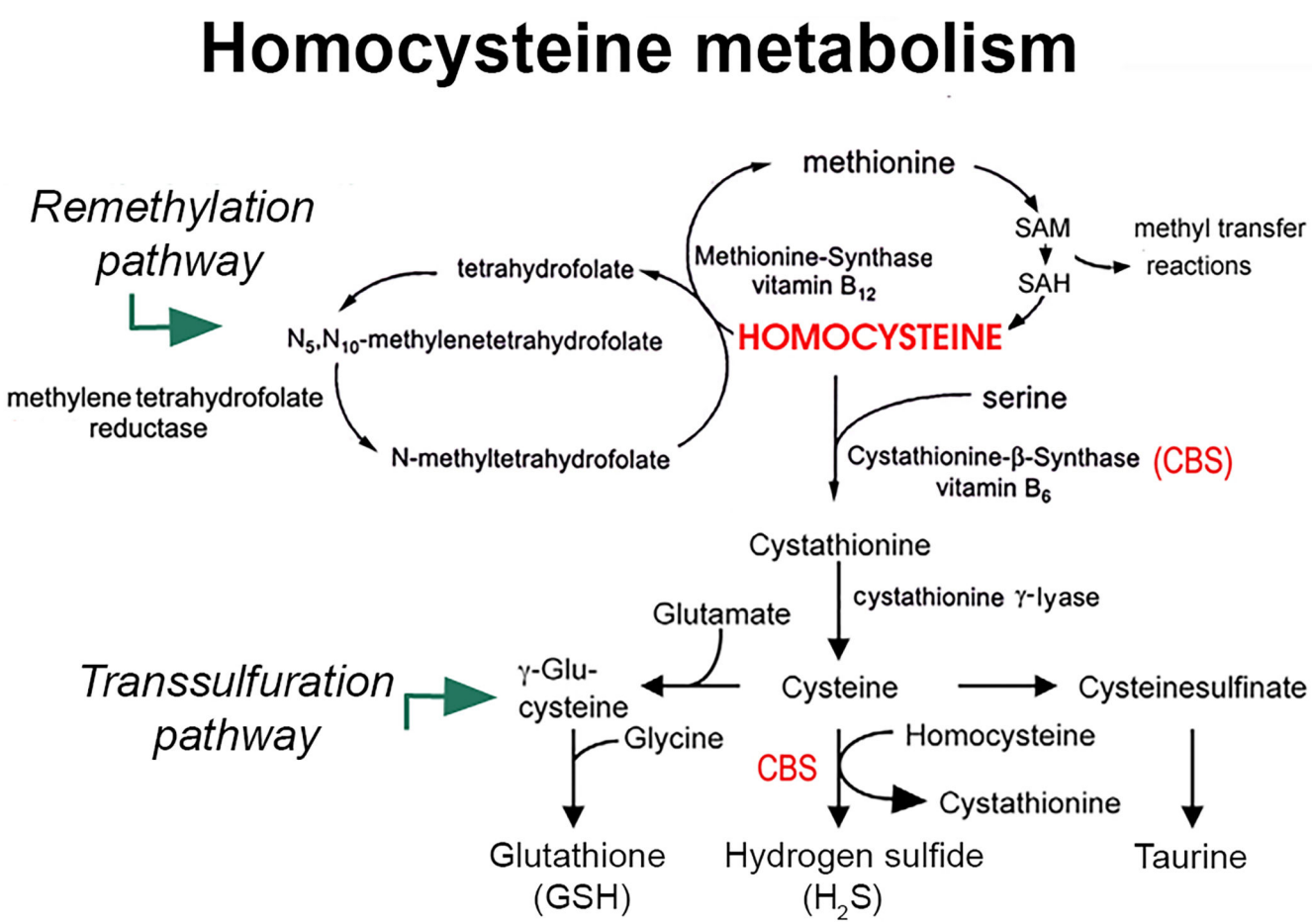

Figure 1. Homocysteine (Hcy) metabolism.

Hcy resides at the intersection of the remethylation and the transsulfuration pathways. In the transsulfuration pathway, excess Hcy is converted to cystathionine in the presence of serine, vitamin B_6 and cystathionine-β synthase (CBS), which is subsequently converted to cysteine via cystathionine γ-lyase. Cysteine is used in the synthesis of glutathione, hydrogen sulfide (H_2S) and taurine. Deficiencies of CBS can lead to hyperhomocysteinemia. Figure adapted from Markand et al, 2015.

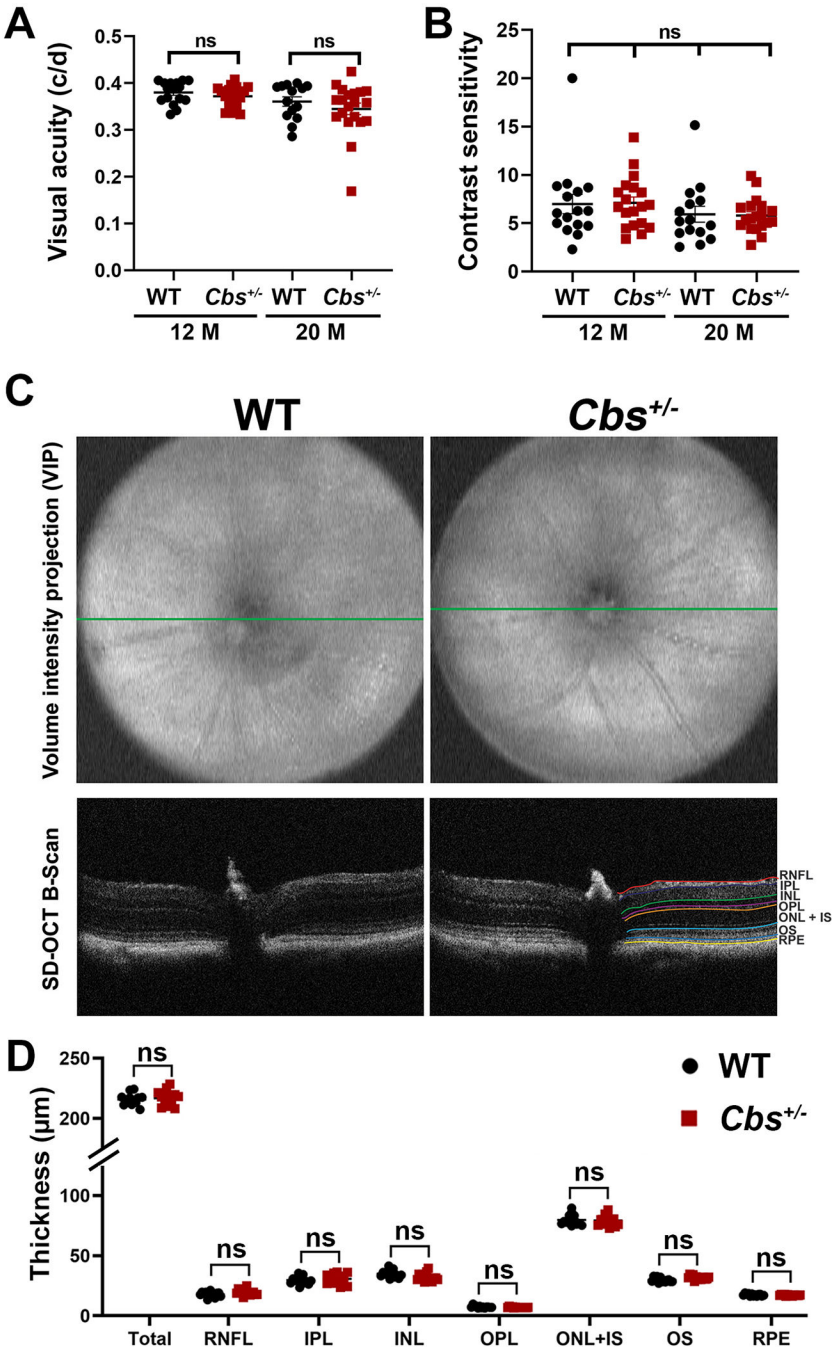

Figure 2. Assessment of visual acuity, contrast sensitivity and retinal structure.

(A) Visual acuity and (B) contrast sensitivity were measured in WT and *Cbs*$^{+/-}$ mice at 12 and 20 months using the OptoMotry apparatus as described. Data are shown for left and right eyes. No significant differences were observed between groups at either age for either assessment. (C) Spectral domain - optical coherence tomography (SD-OCT) was performed in anesthetized 20 month WT and *Cbs*$^{+/-}$ mice to evaluate retinal structure *in vivo*. Representative volume intensity projections and OCT B-scans are shown. (D) Retinal layer thickness was quantified using DIVERS software including total retinal thickness

(total), retinal nerve fiber layer (RNFL), inner plexiform layer (IPL), inner nuclear layer (INL), outer plexiform layer (OPL), outer nuclear layer and inner segment (ONL+IS), outer segments (OS), retinal pigment epithelium (RPE). The right panel "B" scan indicates the guides for each of the retinal layers. Data are shown for the average of both eyes. There were no significant differences in the thickness of any retinal layers analyzed in WT compared to *Cbs*$^{+/-}$ mice. (ns = not significant).

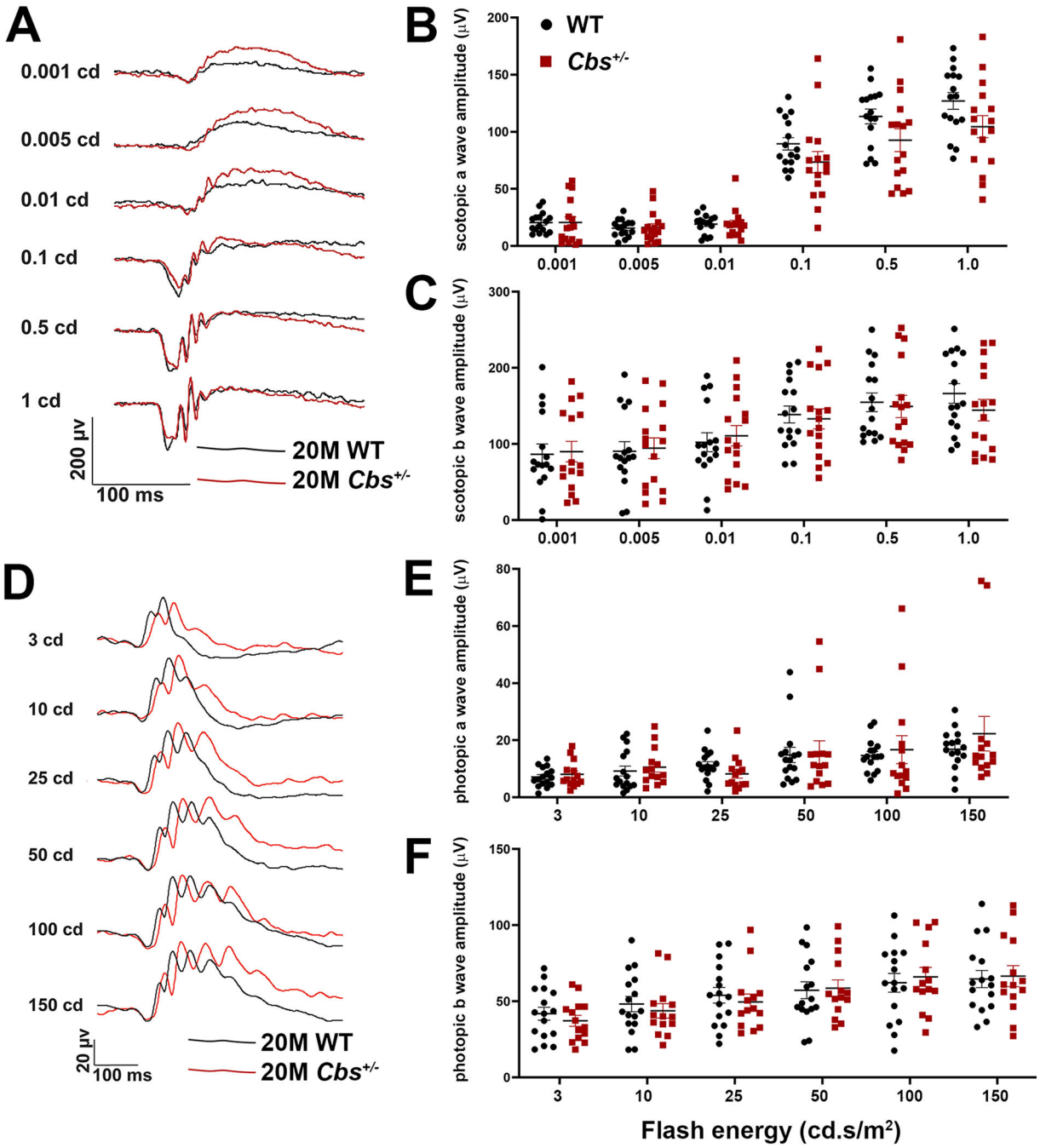

Figure 3. ERG assessment of retinal function.

Assessment of retinal function by dark adapted (scotopic) and light-adapted (photopic) ERG in 20 month WT and *Cbs*$^{+/-}$ mice. Mice were dark adapted and anesthetized as described. (A) Representative scotopic tracings at six flash intensities (0.001 – 1.0 cd.s/m^2) for WT and *Cbs*$^{+/-}$ mice. (B) Scotopic a-wave amplitudes and (C) b-wave amplitudes for both mouse groups plotted at the six light intensities. (D) Representative photopic tracings at six flash intensities (3 – 150 cd.s/m^2) for WT and *Cbs*$^{+/-}$ mice. (E) Photopic a-wave amplitudes and (F) b-wave amplitudes for both mouse groups plotted at the six light intensities. Intensities

were in units of candela-seconds per meter squared (cd.s/m^2). Data in panels B,C,E,F are for left and right eyes. There were no significant differences between groups for rod or cone responses in 20 month old WT versus *Cbs*$^{+/-}$ mice.

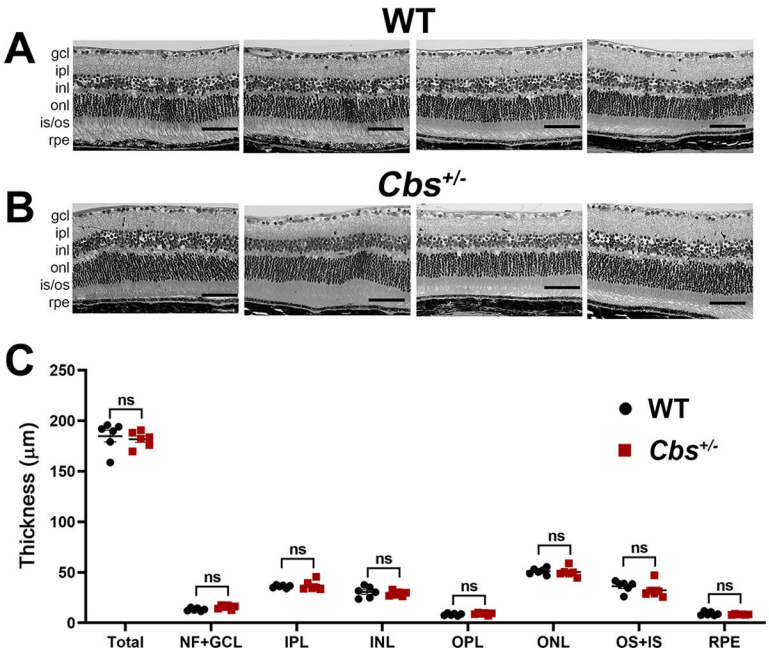

Figure 4. Assessment of retinal histology.

At the conclusion of functional visual assessments, 20 month WT and *Cbs*$^{+/-}$ mice were euthanized and eyes were processed for embedding in JB-4 methacrylate. Representative retinal images of (A) four WT and (B) four *Cbs*$^{+/-}$ mice. Calibration bar = 50μm. (C) Images were subjected to systematic measurements as described and included: total retinal thickness and thickness of nerve fiber & ganglion cell layers (NF+GCL), inner plexiform layer (IPL), inner nuclear layer (INL), outer plexiform layer (OPL), outer nuclear layer (ONL), outer & inner segments (OS+IS), and retinal pigment epithelial layer (RPE). Data are shown for the average of both eyes. No significant differences were observed between groups for any retinal layer. (ns = not significant)

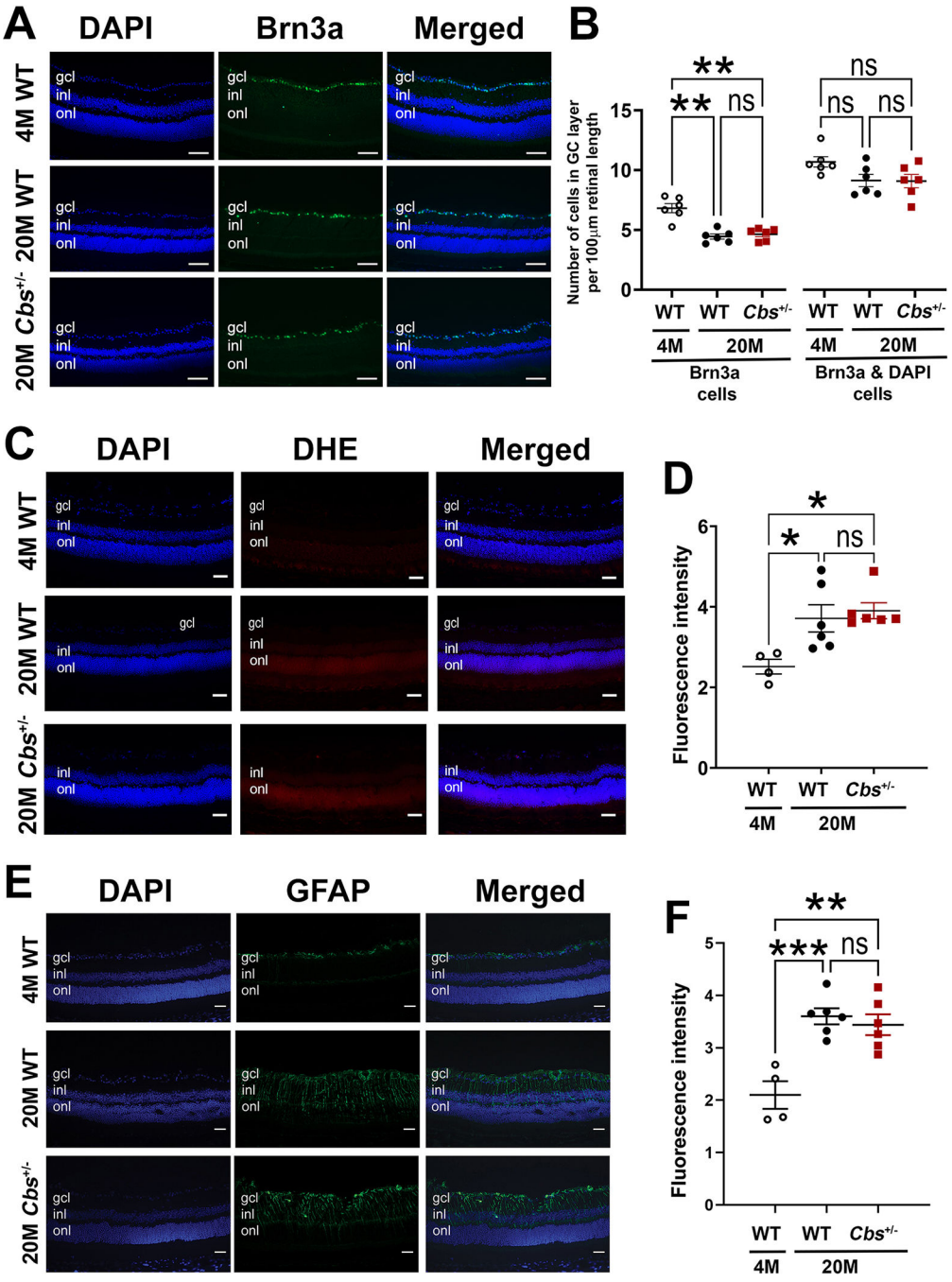

Figure 5. Immunodetection of Brn3a, DHE, and GFAP.

Representative photomicrographs of retinal cryosections from 20 month WT and *Cbs*$^{+/-}$ mice that were subjected to (A) immunodetection of Brn3a (green), a marker of RGCs and DAPI (blue) to label all cell nuclei; (B) quantification of the number of Brn3a-positive RGCs in the central retina as well as the number of Brn3a-DAPI-positive cells; (C) immunodetection of DHE, which fluoresces red upon reaction with superoxide species and serves as a marker of oxidative stress and DAPI (blue) to label all cell nuclei; (D) quantification of DHE fluorescent intensity; (E) immunodetection of GFAP, which

fluoresces green under conditions of gliosis and DAPI (blue) to label all cell nuclei; (F) quantification of GFAP fluorescent intensity. Data shown in panels B,D,F are the average of both eyes and were analyzed by two-way ANOVA, Tukey's multiple comparison test was the post-hoc test. There were significant differences in the number of Brn3a-positive cells as well as fluorescence intensity for DHE and GFAP between retinas of 4 month WT versus 20 month WT and *Cbs*$^{+/-}$ mice (*=p<0.05, **=p<0.01, ***=p<0.001), but no significant (ns) differences between the retinas of 20 month mice in either group. Abbreviations: gcl = ganglion cell layer, inl = inner nuclear layer, onl=outer nuclear layer. (Calibration bar = 50 μm)

Table 1.

Number of animals used in the study.

Mouse Group	*n*	Age (post-natal months)
IOP detection		
WT (*Cbs*$^{+/+}$)	8	12
Cbs $^{+/-}$	11	12
WT (*Cbs*$^{+/+}$)	9	20
Cbs $^{+/-}$	7	20
SD-OCT analysis of retinal structure		
WT (*Cbs*$^{+/+}$)	7	20
Cbs $^{+/-}$	7	20
ERG analysis of retinal function		
WT (*Cbs*$^{+/+}$)	8	12
Cbs $^{+/-}$	9	12
WT (*Cbs*$^{+/+}$)	8	20
Cbs $^{+/-}$	8	20
PERG analysis of retinal function		
WT (*Cbs*$^{+/+}$)	8	12
Cbs $^{+/-}$	8	12
WT (*Cbs*$^{+/+}$)	6	20
Cbs $^{+/-}$	6	20
OMR analysis of visual acuity and contrast sensitivity		
WT (*Cbs*$^{+/+}$)	8	12
Cbs $^{+/-}$	11	12
WT (*Cbs*$^{+/+}$)	7	20
Cbs $^{+/-}$	10	20
Morphometric analysis		
WT (*Cbs*$^{+/+}$)	6	20
Cbs $^{+/-}$	6	20
Immunohistochemical analysis		
WT (*Cbs*$^{+/+}$)	4	4
WT (*Cbs*$^{+/+}$)	6	20
Cbs $^{+/-}$	6	20